AGU100 ADVANCING EARTH AND SPACE SCIENCE

Radio Science

RESEARCH ARTICLE
10.1029/2019RS007012

Key Points:
- Ionospheric tilt measurement is a powerful method to study ionospheric disturbances
- Climatology of middle-latitude TIDs is established
- Daytime TIDs propagate against the neutral wind; nighttime TIDs propagate equatorward

Supporting Information:
- Supporting Information S1

Correspondence to:
V. Paznukhov,
vadym.paznukhov@bc.edu

Citation:
Paznukhov, V., Altadill, D., Juan, J. M., & Blanch, E. (2020). Ionospheric tilt measurements: Application to traveling ionospheric disturbances climatology study. *Radio Science*, *55*, e2019RS007012. https://doi.org/10.1029/2019RS007012

Received 11 OCT 2019
Accepted 24 DEC 2019
Accepted article online 2 JAN 2020

Ionospheric Tilt Measurements: Application to Traveling Ionospheric Disturbances Climatology Study

Vadym Paznukhov[1], David Altadill[2], José Miguel Juan[3], and Estefania Blanch[2]

[1]Institute for Scientific Research, Boston College, Boston, MA, USA, [2]Observatori de l'Ebre (OE), CSIC - Universitat Ramon Llull, Roquetes, Spain, [3]Research Group of Astronomy and Geomatics, Universitat Politècnica de Catalunya, Barcelona, Spain

Abstract Ionospheric tilt is a concept used to characterize local horizontal electron density gradients in the ionosphere using a mirror reflection model. Experimental results are presented that illustrate the validity and accuracy of such approach. Analysis of the tilt measurements collected in 2012–2014 with a digisonde at Ebro observatory (40.8°N, 0.5°E) is presented. Digisonde systems allow measuring angles of arrival of ionospherically reflected radio signals, from which the ionospheric tilts are derived. The tilts are represented in terms of North-South and East-West components. Using several years of observations, a climatological distribution of wavelike variations in the tilt records presumed to be associated with traveling ionospheric disturbances (TIDs) is established. Most of the observed TIDs have their main periods of 30 min to 1.5 hr which is rather typical for medium-scale TIDs. Summertime appears to have the most frequent occurrence of TIDs. There is a good agreement between the presence of TIDs and sporadic E layer occurrence, suggesting that some TIDs can be driven by instability in the electric field which is initiated via an interhemispheric link between the E and F regions of the ionosphere. Direction of disturbance propagation is also analyzed and compared to the modeled neutral wind. There are indications that during the daytime TIDs tend to propagate in the direction opposite to the background neutral wind. This suggests that daytime TIDs are produced by atmospheric gravity waves originating in the lower atmosphere and experiencing background wind filtering effect on their upward propagation.

1. Introduction

Plasma density distribution in the Earth's ionosphere is highly inhomogeneous, that is, it varies significantly with height, latitude, and longitude. Therefore, at each point in space, the state of the ionospheric plasma is characterized not only by the ambient scalar density but also by a density gradient vector. Ionospheric gradients can be roughly divided into two groups: synoptic and dynamic gradients. The former is the result of a combination of the major processes controlling ionospheric plasma dynamics: photoionization, recombination, and transport. Thus, in general, the ionosphere in polar regions has significantly lower densities than at the equator, and, therefore, there is a permanent synoptic gradient towards the equator in middle latitudes. As of today synoptic gradients in general are well understood and can be successfully modeled with empirical or physics-based ionospheric models, for example, International Reference Ionosphere (Bilitza et al., 2017), Parameterized Ionospheric Model (Daniell et al., 1995), and so forth. Dynamic gradients are typically associated with the small-scale ionospheric inhomogeneities, for example, traveling ionospheric disturbances (TIDs), polar patches, spread-F disturbances, and others. There are also very important gradients associated with the solar terminator, which occur regularly, and were also shown to produce propagating waves in the ionosphere (Galushko et al., 1998; Somsikov, 1987).

Since these are all transient phenomena, they are difficult to observe, classify, and model. Detecting ionospheric gradients is a challenging task since it requires the use of techniques that allow establishing ionospheric density distribution not only as a function of time but also as altitude and/or latitude and longitude (e.g., Jakowski et al., 2008). Ideally, a full 3-D distribution of ionospheric plasma needs to be measured. Current data-assimilative ionospheric models, like IRTAM (Galkin et al., 2012), EDAM (Angling et al., 2009), and RTIM (Barnes et al., 2000), can estimate such a 3-D plasma distribution. However, only large-scale gradients can be captured by these models. Most ionospheric remote sensing as well as in situ techniques do not provide full ionospheric characterization. However, as discussed in section 2, some advanced ionospheric sounders (i.e., digisondes; Reinisch et al., 2009) allow detecting ionospheric gradients under some simplifying assumptions.

Ionospheric gradients are especially important for High Frequency (HF) geolocation applications, in which angles of arrival (AoAs) are used to determine the position of the targets. The knowledge about the presence of gradients becomes critical for the accurate location of the targets.

Research into physics and phenomenology of TIDs is a popular subject in ionospheric community. First, TIDs can travel over large distances, thus affecting large areas of the ionosphere. Second, TIDs are very common phenomena, occurring routinely over a wide range of geographic latitudes.

Although TIDs were first observed several decades ago, during the rise of the ionospheric science (e.g., Munro, 1950), even today a lot is still unknown about the physics and climatology of these waves. Conventionally, TIDs are divided into two major classes: large-scale TIDs (LSTIDs) with wavelengths over 1,000 km and medium-scale TIDs (MSTIDs) with shorter wavelengths. LSTIDs are mostly associated with the disturbances originating in the polar region during the major geomagnetic storms (e.g., Pradipta et al., 2016, and references therein) and produced by energy input from the magnetosphere. The two major natural sources of MSTIDs are atmospheric gravity waves (AGWs) (e.g., Hooke, 1968) and disturbances in electric field, producing the so-called electrified MSTIDs (e.g., Narayanan et al., 2018). AGWs which are the oscillations of neutral atmospheric gas can themselves be produced by a wide variety of sources, both natural (meteorological/tropospheric phenomena) and artificial (e.g., powerful explosions). Many studies dedicated to TID observations, measuring their characteristics and establishing their climatology and origins, have been carried out, spanning from the equator to high latitudes (Bauer, 1958; Bishop et al., 2006; Georges, 1968; Hocke & Tsuda, 2001; Hung et al., 1978; Kelley, 1997; Korepanov et al., 2009; Röttger, 1977; Sauli & Boska, 2001; Vadas & Crowley, 2010; Waldock & Jones, 1987; Yampolski et al., 2004). Several authors tried modeling TID propagation and signatures they produce on the HF radar observations (e.g., Cervera & Harris, 2014). Although significant advances in our understanding of TIDs have been made to date, a complete picture is yet to emerge. This is why research into TID phenomena is still an important topic for the ionospheric community.

2. Ionospheric Tilt Measurements

The digisonde at Ebro station in Spain (geographic coordinates: 40.8°N, 0.5°E; geomagnetic coordinates: 43.0°N, 81.5°E) routinely makes ionospheric observations which consist of vertical ionograms and skymap measurements made at several fixed frequencies. It is also worth noting that since 2017, the Ebro digisonde has been routinely supporting oblique bistatic measurements with the Dourbes system in the framework of the Net-TIDE project (Reinisch et al., 2018). Ionograms make it possible to determine the state of the "background ionosphere" by inferring vertical electron density profile using ARTIST and NHPC tools (Reinisch et al., 2005). Skymap measurements are made in order to observe the presence of irregularities and to determine plasma drifts. The transmitted signal illuminates a large area in the ionosphere, typically a few hundred kilometers in diameter. At the point where the local index of refraction becomes equal to zero, the sounding pulse is "reflected" from the ionosphere. If the normal to the surface of equal electron density contour points exactly towards the sounder, then the reflected signal returns to the sounder. Each such reflection point can be considered as a "source" of reflected signal. A map showing locations of all such "sources" is called a "skymap" (Figure 1, right panel). From the collection of the sources in the skymap the orientation of the normal vector characterizing the ionospheric tilt of an imaginary reflecting plane can be derived (Kozlov & Paznukhov, 2008). In essence, this approach assumes a mirror type reflection of HF waves, a very simple model that neglects refraction from underlying layers and consider a flat Earth/ionosphere reflection geometry, which nonetheless can be efficiently used to characterize HF wave reflections from the ionosphere as long as magnetic field effects are not very strong (Dao et al., 2016; Huang et al., 2016; McNamara, 1991). Skymap soundings are made at several frequencies selected to match approximately to the middle of the F trace at 5 min sampling.

The validity of the tilt concept and mirror reflection model is illustrated with the following experimental results. We used oblique sounding data collected on a dedicated bistatic HF link deployed in New Mexico, United States, under the IARPA high-frequency Geo program (Munton et al., 2019). The operating frequency was 5.4 MHz, and the receiver was located about 100 km North of the transmitter, continuously recording AoAs among other signal trajectory parameters. There was a single digisonde station near the midpoint of the HF link, making skymap measurements every 2 min, from which tilt vectors were calculated.

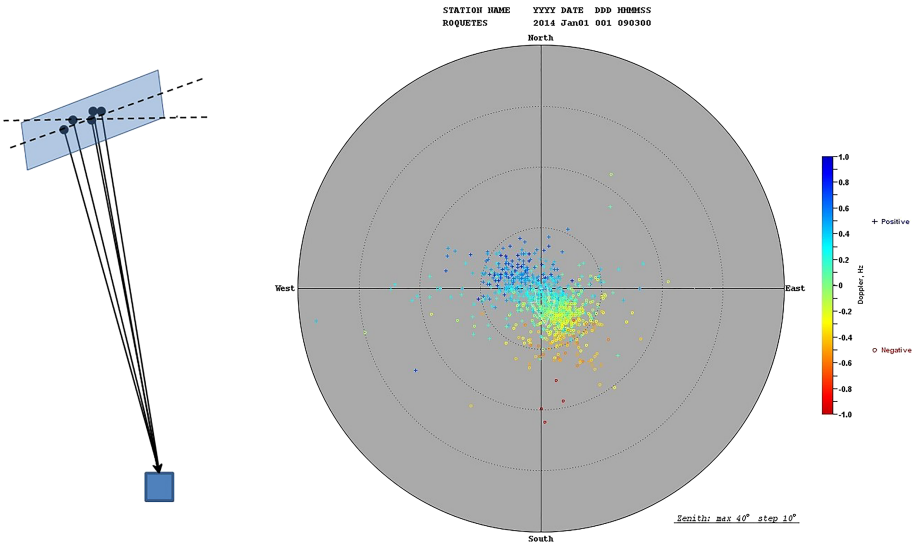

Figure 1. Ionospheric tilt angles specify the orientation of an imaginary surface which reflects radiowaves to produce a specific skymap. Tilt angles are found as a "center-of-mass" of all the sources present in the skymap data.

Using the midpoint digisonde tilt measurements and the known geometry of the experiment, we calculated the expected AoA variations at the receiver (with the mirror reflection model) for the specific experiment on 19 January 2014. This comparison is shown in Figure 2 where one can see an excellent agreement between the measured (blue) and derived (black) variations of azimuthal and elevation angles. In this case the observed wavelike variations in AoAs are most likely produced by the traveling ionospheric disturbances passing over the midpoint of the radio link. Note that the dominant period of the wavelike observations is about 30 min, although it does vary over the time interval of observations. The amplitude of the variations also fluctuates on this time scale. This AoA modeling has been made with the reflection height fixed at 250 km according to the ionospheric conditions determined from the ionogram measurements (not shown). In reality, of course, the height of the reflection also varies following changes in the background ionospheric plasma.

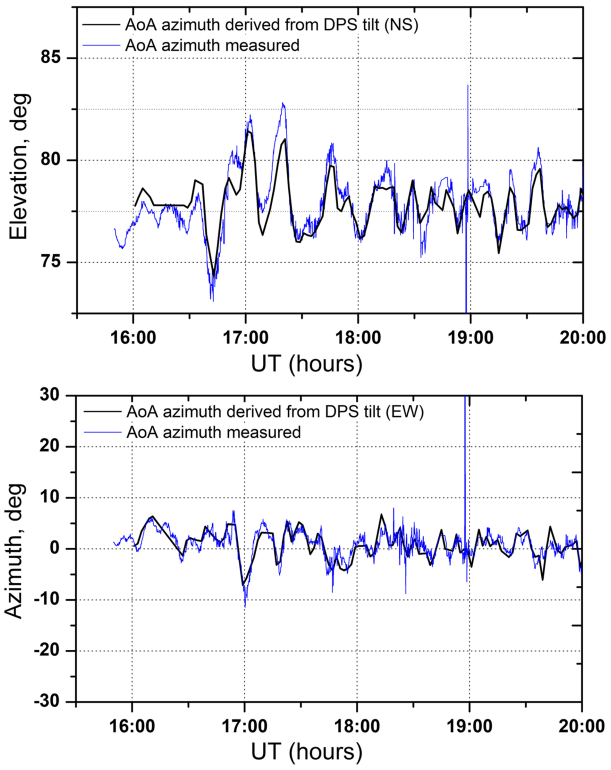

Figure 2. Using ionospheric tilt measurements near the midpoint of an HF link, it is possible to calculate corresponding AoAs at the receive location. Top plot compares elevation angle measurements (blue) and modeling (black), and bottom one shows azimuthal angle comparison. This example shows AoA modeling with the use of the mirror model reflection and with the fixed reflection height at the midpoint, estimated from simultaneous ionogram measurements.

This validation test (although not made directly at the Ebro digisonde) confirms the feasibility of the digisonde tilt measurements and applicability of the mirror reflection model to the first degree.

We also made a comparison of the tilts derived from digisonde at Ebro and those deduced from GNSS Total Electron Content (TEC) measurements, which is of general interest for the ionospheric community studying disturbances in the ionosphere. Of course, TEC data cannot provide a direct measure of the ionospheric tilts as they produce an integrated electron content along the line of sight from the TEC receiver to the GPS satellite. TEC values are normally calculated using phase difference between the signals traveled through the ionosphere at different frequencies and assuming a single thin layer model for the ionosphere with a fixed height (e.g., Hernández-Pajares et al., 2009). However, in the regions with dense GNSS networks, for example, Europe, it is possible to avoid using single layer model and to separate the ionospheric delays occurring in the top and bottom parts of the ionosphere (Rovira-Garcia et al., 2016). Thus, we can concentrate on wavelike processes in the lower part of the ionosphere which are especially suitable for the comparison with HF observations. By using a network of closely located stations, it is possible to

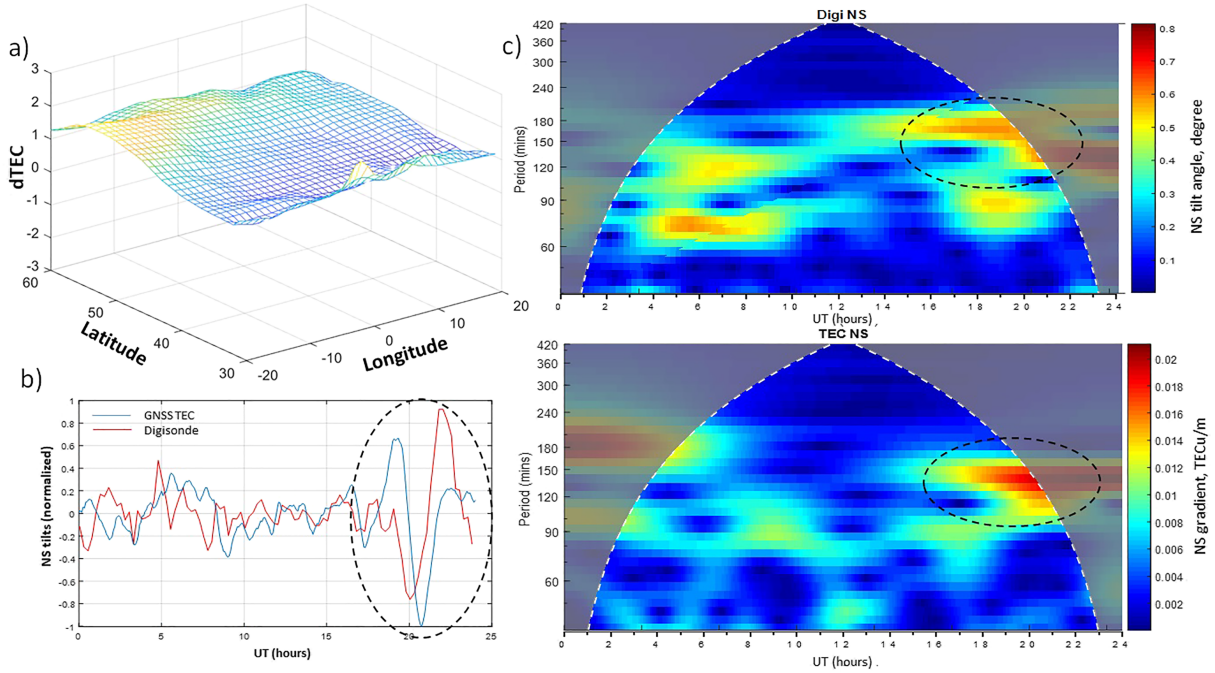

Figure 3. Comparison of the tilts derived from digisonde and GNSS TEC measurements. Figure 3a shows an example of the bottomside TEC map (effective surface) calculated using the network of the GNSS TEC receivers with the central point above Ebro Observatory. This snapshot is made for 21.9 UT on 23 April 2014. Figure 3b shows a comparison of the North-South normalized tilt components calculated from the TEC map and measured with the Ebro digisonde. Figure 3c compares the wavelet power spectrum for North-South tilt components measured with the Ebro Digisonde (top) and calculated from the TEC map (bottom).

calculate a distribution of the electron density within certain geographical region and to determine the presence of horizontal gradients. For the purpose of comparison to the digisonde tilt measurements, this TEC distribution in horizontal direction can be represented as an effective surface whose vertical displacement corresponds to the change in the TEC values with respect to a certain reference level. Using such effective surface representation of the TEC distribution, ionospheric tilt can be calculated as the surface normal vector at any given location. Comparison of the effective tilt from TEC data and digisonde tilt measurements at Ebro location is shown in Figure 3. Raw GPS data used for this calculation were downloaded from ftp://cddis.gsfc.nasa.gov/pub/gps/data/daily/. The TEC effective surface snapshot shown in Figure 3a is made at 21.9 Universal Time (UT) on 23 April 2014. Note the very strong large scale wave, which is oriented along the meridian. A movie provided as supporting information (Movie S1) allows seeing the actual propagation of the disturbance. Figure 3b shows a comparison of the North-South (NS) tilt components (normalized) which are calculated from the TEC map and measured with the Ebro digisonde on this day. Although the agreement is not perfect, one can see that both techniques respond to the presence of the disturbances in a similar fashion, best matching during the presence of the strong wave observed at the end of the day. There is an interesting phase offset between the digisonde and TEC measurements, which may arise due to the height differences. Indeed, digisonde measurements are made at the F-region heights, below the main ionospheric peak, while GNSS TEC is integrated over all heights, but as mentioned, most of the contribution into the vertical TEC comes from the topside ionosphere. Thus, the observed offset in the measured tilts/gradients could be indicating the presence of the vertical component of the propagation velocity or a slanted phase front. The agreement between the two measurements is also illustrated with the wavelet plots shown in Figure 3c. Although the digisonde measurements (top) show more spectral features of the variations than GNSS data, both observations show the presence of the waves with similar periods, and the strongest disturbance observed near the end of the day shows the same periodicity in the wavelet plot (highlighted in the figure).

Although strong events compare reasonably well, as shown in Figure 3, statistically, however, the agreement between the two methods is rather fair. Using almost a month of data, we calculated a correlation coefficient between two measurements within 3 hr long sliding window, and found that its value rarely exceeds 0.5, which usually corresponds to the presence of very strong variations. This result should not be very

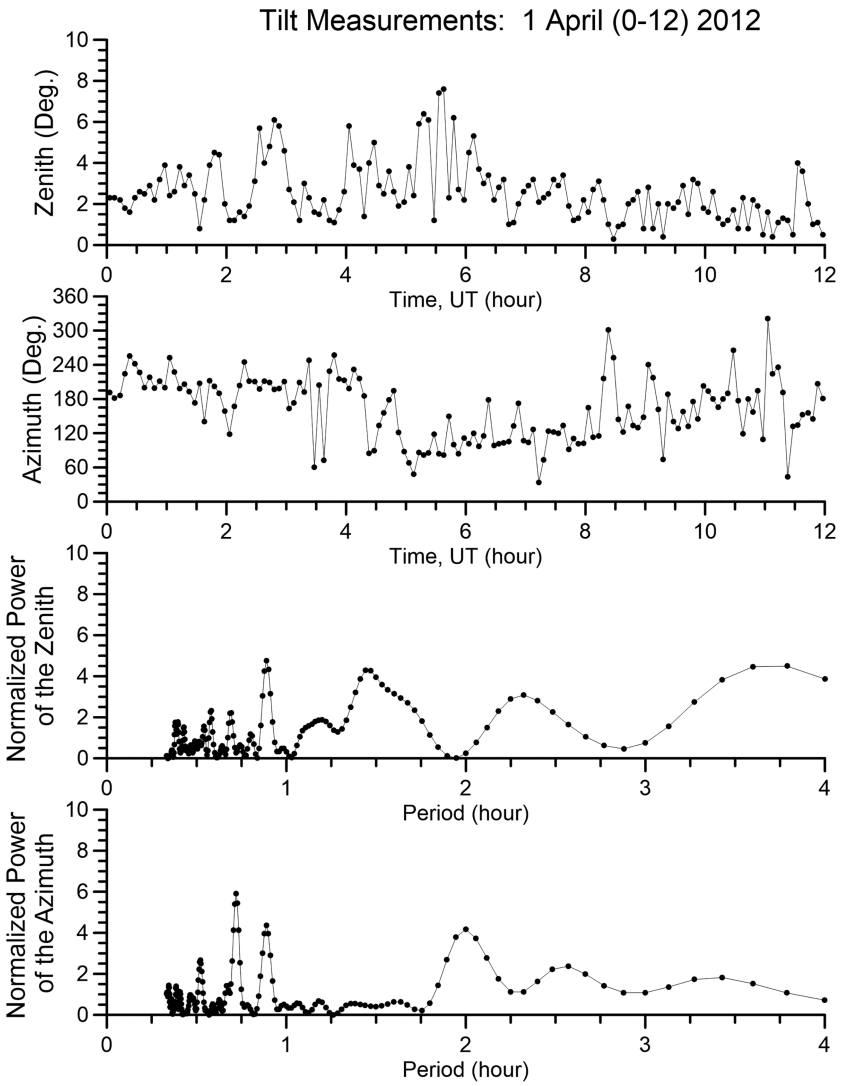

Figure 4. Example of routine tilt measurements at Ebro station. The top two panels show zenith and azimuth angle that characterize the tilt, that is, the position of the normal vector. Two bottom panels show an example of spectral analysis (normalized power) of the zenith and azimuth variations.

surprising, given the integrated kind of measurements that are provided by the GNSS TEC method. Nevertheless, the simultaneous presence of the wavelike variations with the same periods suggests that both methods are capable of detecting wavelike disturbances and identifying their periods at least under the quasi steady state conditions of the background ionosphere.

3. Tilt Data Collection

Figure 4 shows an example of routine daily tilt measurements at Ebro station. Raw ionosonde data used in this study are available from UMass Lowell database: https://ulcar.uml.edu/DriftBase/. The top two panels show zenith and azimuth angles that characterize the tilt, that is, orientation of the normal vector. In further analysis, we prefer using Cartesian projections of the normal vector (North-South and East-West) which are more continuous and smooth functions of time. Two bottom panels show examples of spectral analysis of zenith and azimuth variations with Lomb-Scargle method (e.g., Hocke, 1998). The raw data can be quite noisy, so a statistical analysis of the data is the most appropriate. The Lomb-Scargle method allows selecting spectral components which are statistically significant. In the given example, several peaks are present in the

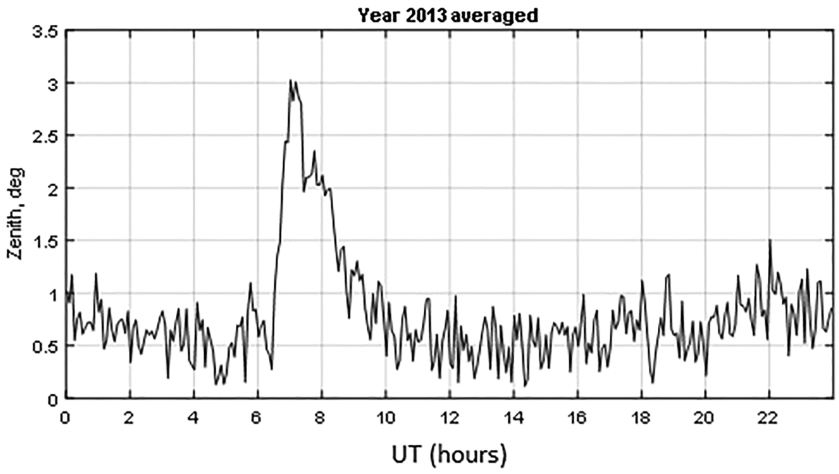

Figure 5. Yearly averaged zenith angle for 2013. It is interesting how strong the zenith variations are during the sunrise, both in absolute value and in comparison to practically absent variations at sunset.

spectra corresponding to wide frequency range; however, we concentrate on the periods below 2 hr which are usually attributed to the traveling ionospheric disturbances rather than to long period tidal waves.

Figure 5 shows a yearly averaged zenith angle measurement from 2013. It is interesting that the effect of the sunrise terminator (around 07 UT on average) is much more pronounced than that of the sunset one. This is probably due to the fact that the increase in the electron density due to the photoionization at sunrise is much more rapid than plasma depletion due to recombination which occurs after the sunset. It is interesting to note that the value of the zenith tilt angle associated with the solar terminator can reach as much as several degrees. Thus one might expect that the accuracy of AoA measurements (critical for HF geolocation systems) is the worst at sunrise because of the presence of very large variations in the angles of arrival caused by the presence of terminator tilts.

Because of the presence of strong regular variations in the tilt angles we selected wavelet analysis to search for the patterns in the tilt variations and associated wavelike processes. Data analysis using wavelet transform has an advantage of eliminating the need for detrending procedure, which is often quite subjective and ambiguous process often leading to creating artifacts in the analyzed data series.

4. Results and Discussion

Availability of the long-term data collection made at Ebro digisondes makes it possible to investigate the climatology of the ionospheric disturbances manifesting themselves as wavelike variations in the tilts. We have analyzed continuous records of ionospheric tilts for the full year of 2012. As mentioned, it is preferable to separate zenith and azimuthal tilt angles into "Cartesian" North-South and East-West angle projections. These two parameters do not experience jump-like changes which are typical of azimuthal angle when it is measured for near vertical directions. Of the two tilt components, naturally, the NS is the one less affected by the terminator gradients, so it was selected for the climatological analysis.

One of the particular reasons we have chosen the year 2012 was that it was quiet enough in terms of geomagnetic activity. Although 2012 was close to the peak of the last solar cycle, there were many more quiet days than disturbed. Thus there was no need to separate quiet and disturbed days to look at the disturbance climatology.

Figure 6 shows monthly averaged continuous wavelet transforms from the NS tilt measurements for February, May, August, and October of 2012, which are representative of four seasons. This kind of representation allows discovering daily distribution and the periods of the quasiperiodic variations present in the tilt records. Thus, it is possible to see the difference in the periods and time of the occurrence of disturbances with different spectral characteristics.

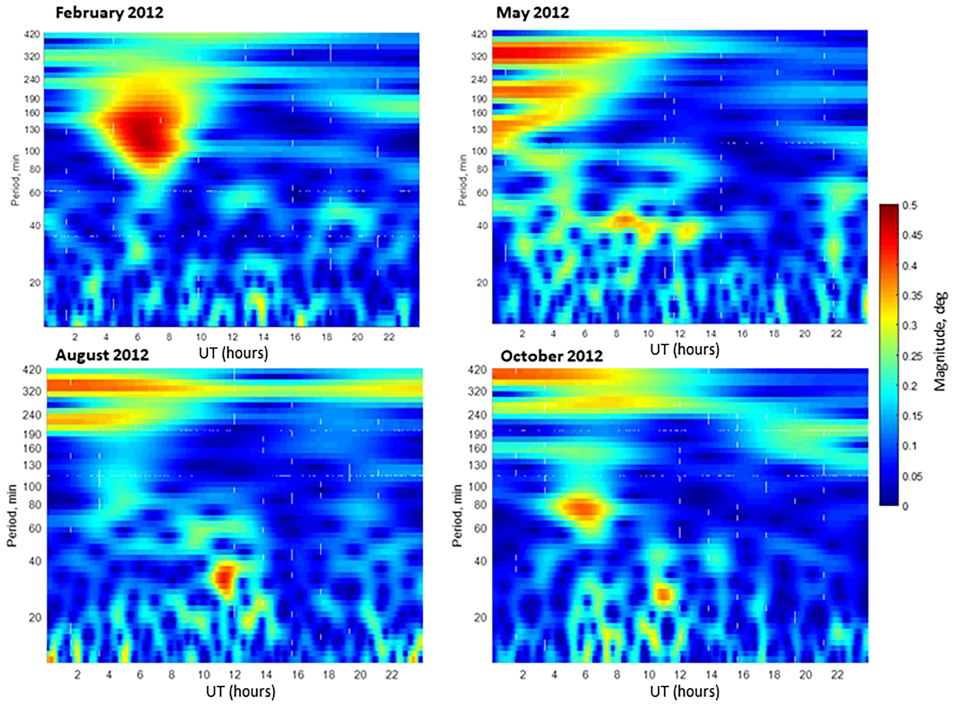

Figure 6. Wavelet analysis of the tilt variations. In this figure, the North-South tilt component is analyzed with continuous wavelet transform showing the intensity (color) of the periodic processes. The panels show monthly averaged variations for four seasons in 2012. The long period waves (>80 min) centered at 06 UT are likely associated with the sunrise effect, while shorter periods may be attributed to the traveling ionospheric disturbances. The climatology of the variations changes significantly throughout the year, but most of the short period processes seem to be observed near summer at daytime; for example, May panel at 08–13 UT with 40 min and August panel at 11–12 UT with 30–40 min.

The long period amplitude enhancement (over 80 min periods) centered at 06 UT are likely associated with the sunrise effect, while shorter periods may be attributed to the traveling ionospheric disturbances. The climatology of the variations varies significantly throughout the year, but most short periods (faster than 80 min) seem to be observed during the summer time maximizing at around 12 UT (at Ebro station, Local Time differs from UT by 2 min only), whereas longer periodic variations tend to occur by night. It is also interesting that the most intensive daytime variations have somewhat longer periods in May (~40 min) which becomes shorter (~30 min) in August and October. February appears to be the quietest month in terms of the disturbance presence.

We also compared disturbance morphology from different years, as shown in Figure 7. Apparently there is no clear relationship between the intensity of the variations and the solar flux (characterized by sunspot number), indicating that most of the observed variations most likely do not have geomagnetic origin, that is, not produced by energy inputs in the auroral region. It is worth mentioning at this point that further future work is needed to address such an analysis over a broader period as new measurements are being provided. Simultaneous ionogram observations from the Ebro digisonde also make it possible to assess background ionosphere density distribution for the period of interest using critical F layer frequency foF2. These data for each year in study are presented in the bottom row in Figure 7. It is evident that at this scale of sun spot number variations (sun spot numbers 55–120) observed between the three years there is no dramatic difference in background plasma densities.

Therefore, the difference in seasonal occurrences of the disturbances is unlikely to be attributed to the background ionospheric plasma distribution either. The relation between the TID occurrence and background plasma characteristics is discussed again in Figure 8 and accompanying text.

Next, we concentrated on the variations with the periods of 20–80 min, which are typical for MSTIDs of both AGW and electric field oscillation origins. The intensity of the disturbances was calculated by averaging the wavelet amplitudes within 20–80 min band and plotting the amplitudes as functions of time and day of year

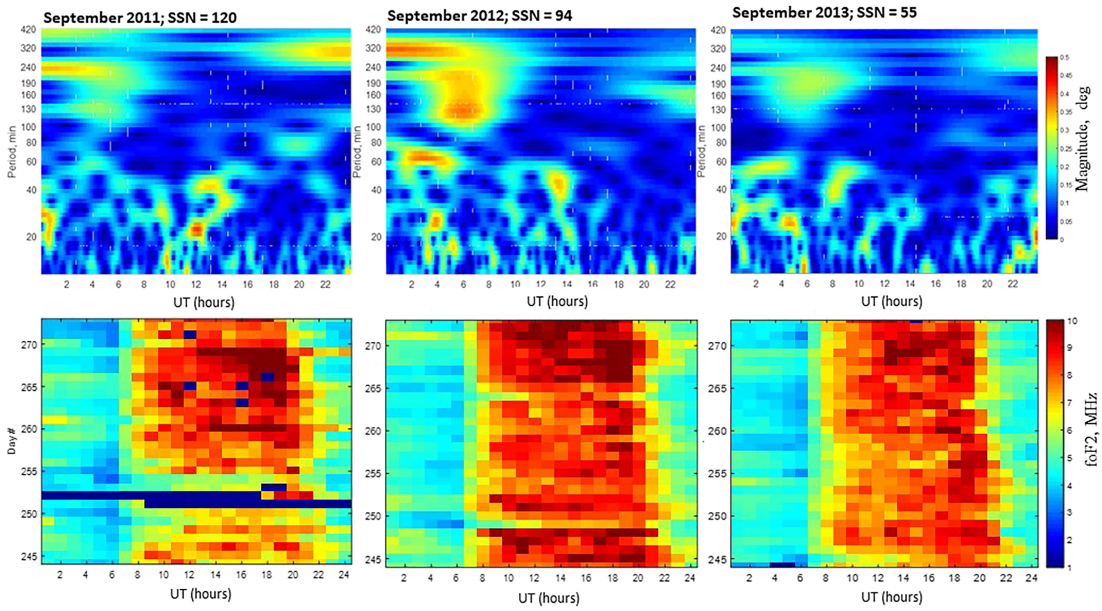

Figure 7. Comparison of the tilt variations (North-South component) for different levels of solar activity during 2011–2013. Top row shows disturbance periods as a function of time a given month, bottom row shows corresponding background density distribution (in terms of foF2). There is no clear relationship between the intensity of the variations and the sun spot number (SSN), indicating that most of the variations are not of geomagnetic origin.

as shown in Figure 8. In order to help distinguishing daytime and nighttime intervals, the sunrise and sunset times (at ground level) for Ebro station are also shown for the entire year.

This resulting pattern is compared to the yearly distribution of the background plasma and occurrence of sporadic E layer shown in the middle and bottom panels correspondingly.

Again, there seems to be no apparent link between the disturbance occurrence and background plasma density as the amplitude of daily maxima of electron density do not change significantly through the year. Summertime and wintertime background density are mainly different by the length of the high-density period, which is naturally the longest during the summer and the shortest during the winter. However, there is a noticeable link between the wavelike disturbance occurrence distribution and sporadic E layer presence. Both the disturbances and sporadic E layer are most frequently observed in the summertime (Days 150–250) and during the daytime as well as shortly after the sunrise. The Perkins instability which gives rise to electrified MSTIDs is formed through the coupling between E and F-region ionospheres in the presence of sporadic E layers (e.g., Cosgrove & Tsunoda, 2004). However, in the ionosphere the E and F regions are also coupled to the conjugated regions in the other hemisphere which complicates the process of instability formation. Narayanan et al. (2018) suggested a mechanism for the link between the nighttime electrified TIDs and sporadic E layers present at both the observation point and the magnetically conjugated point. It was shown that presence of strong sporadic E layer at any of the two conjugated regions is sufficient to give rise to the electrified TIDs. Although we do not have observations from the conjugated location, our simultaneous observations of sporadic E layer and TIDs at Ebro observatory tentatively confirm the proposed scenario. Again, further investigation with larger period of analysis are needed to confirm the Cosgrove and Tsunoda (2004) electrified MSTID mechanism. It is also interesting that a similar link is present during the post sunrise period when the electrified MSTIDs are not expected to be present. This effect needs further investigation. It is worth noting that other researches also suggested sometimes peculiar connections between sporadic E layers and ionospheric irregularities. Batista et al. (2008) observed a correlation between sporadic E layer and spread F in South American sector. Zalizovski (2008) observed a positive correlation between the tropospheric disturbances and sporadic E layer in Antarctica. Although in the latter study, the exact physical mechanism of the correlations was not defined, it is possible to speculate that tropospheric disturbances may produce both the sporadic E enhancement and the TID disturbances at the F-region heights. Of course, a detailed investigation with convincing case studies is needed to see if this suggestion

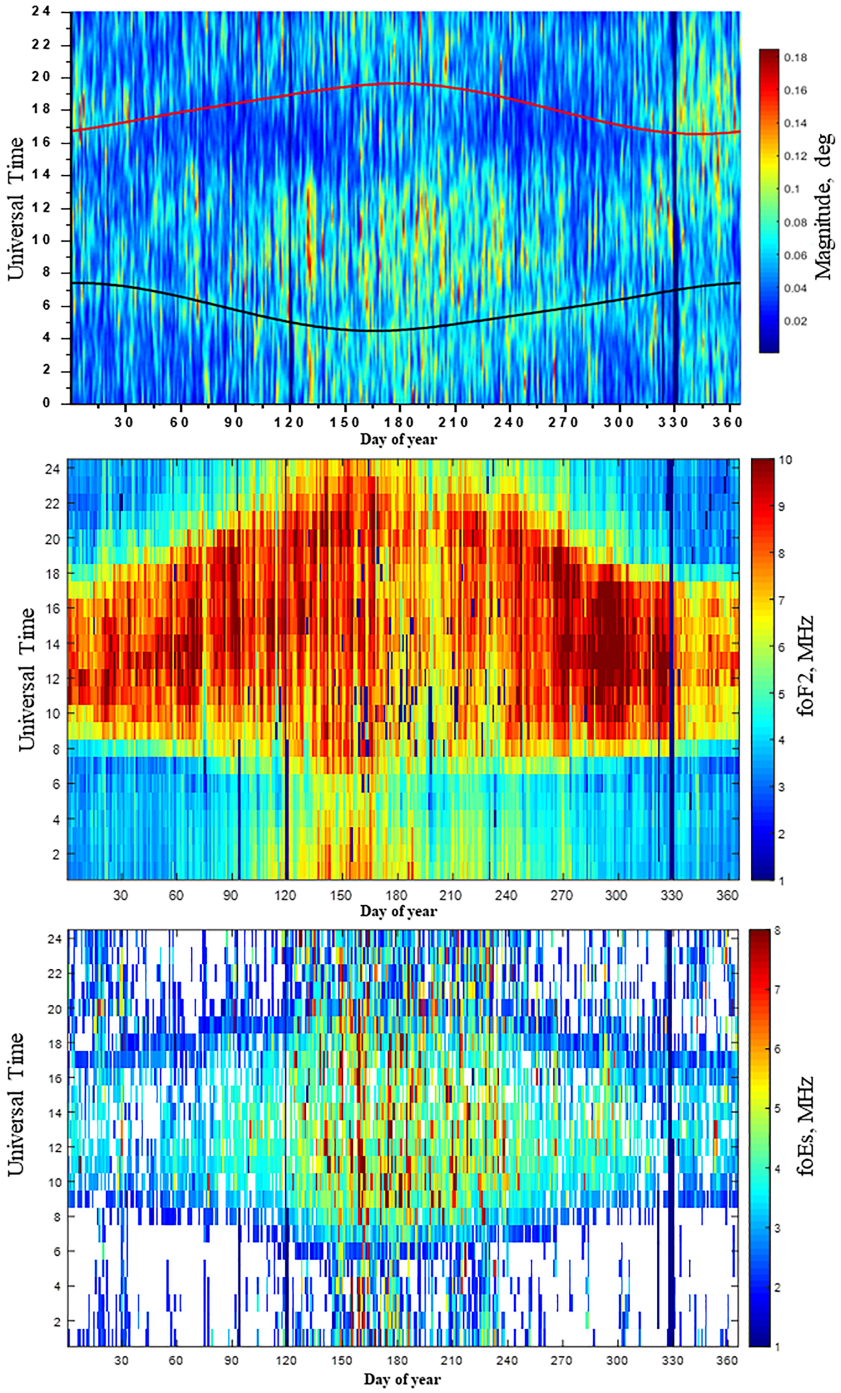

Figure 8. Top: climatology of short period (20–80 min) variations for North-South component calculated for 2012. The black and red lines indicate the sunrise and sunset times (at ground level) correspondingly. Middle: plasma density distribution in terms of critical frequency, foF2. Bottom: sporadic E layer occurrence at Ebro, showing the strongest sporadic layers present during the summertime period.

may be sustained. But if found feasible, this suggestion may explain the observed relationship between the sporadic E layers and F-region disturbances observed in our data during the daytime.

To investigate further the relation between the F-region disturbances and the lower atmosphere processes, we looked at the direction of propagation of the disturbances. Although with a single point observations like

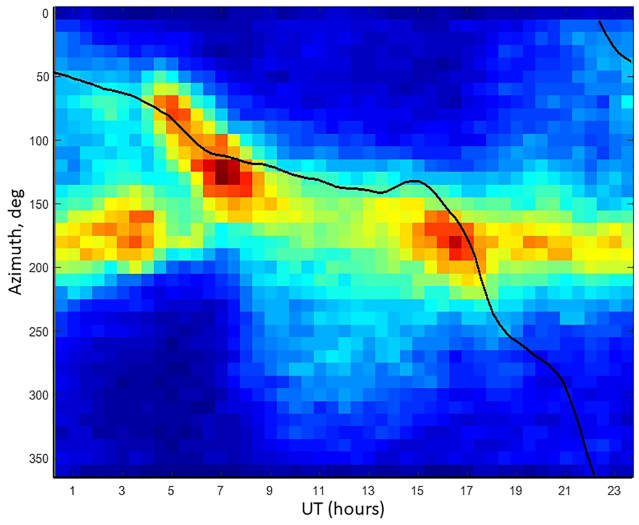

Figure 9. Distribution of the measured tilt azimuth (colormap) compared to the direction opposite to the neutral wind velocity (black line) for the year 2013. Azimuth is counted clockwise from the true north direction. Azimuthal direction of the tilt angle can be regarded as an indicator of the TID wave propagation direction (under the assumption of the TID plane wavefront). Neutral wind direction is calculated with TIEGCM model.

the ones from an isolated digisonde it is difficult to accurately measure parameters of ionospheric waves, under some simplifying assumptions it is possible to do so.

It has been shown that it is possible to infer TID parameters from digisonde skymap measurements using a simplified model for TIDs, for example, plain waves represented by a perfectly reflecting surface (Obenberger et al., 2019; Paznukhov et al., 2012). However, no direct measurements of tilt angles are used in that approach. In this work we wanted to establish a characteristic distribution of the ionospheric tilts/gradients and to establish if it can be used to characterize TIDs. As discussed above the orientation of the tilt normal vector represents a perpendicular to the "imaginary" ionospheric plane or local electron density contour. If we assume that most off-zenith reflections are associated with the propagating disturbances which in the case of the TIDs are characterized with the plane wavefront, then the azimuthal direction of the tilt vectors characterizes the propagation direction of the TID waves. Of course, this is valid only under the assumption of the mirror model reflection or in other words, free-space propagation. However, our validation test results presented in Figure 2 can be used to justify such approach. Moreover, the North-South and East-West tilt components when converted to zenith and azimuth angle show a rather consistent direction, with a minimal number of points with 180° azimuth ambiguity which are easily removed as outliers. It should be noted that the instrumental biases resulting from the finite phase differences between digisonde receive channels that produce constant tilt offsets were removed before the processing of all data volume.

Figure 9 shows a yearly averaged azimuth direction of the tilts for year 2013. Azimuthal distribution is shown as a function of time, with the color indicating the percentage/number of observations within each 10° bin for each 30 min time stamp. The resulting azimuthal distribution is compared to the neutral wind velocity calculated using TIEGCM model for Day 155. The black curve in the plot actually shows azimuthal direction opposite (shifted by 180°) to that of the modeled neutral wind to better observe the potential link between both the neutral wind direction and dominant azimuth direction of the tilts. It is interesting that there is a reasonably good agreement between the neutral wind and averaged tilt azimuth during the period of 05–18 UT which represent a daytime (see Figure 8 for the changes in sunrise/sunset times during the year). The high similarity between the neutral wind direction and tilt azimuth distribution indicates a possible "wind filtering" effect, suggesting the measured tilt azimuth is indicative of the ionospheric waves that during the daytime are produced by AGWs originating in the lower atmosphere.

It has been suggested that tropospheric AGWs propagating upward interact with the horizontal background wind in the mesosphere, which results in severe attenuation of the wave amplitude depending on the direction of the wave propagation with respect to the wind (e.g., Taylor et al., 1993). This effect is conventionally called "wind filtering" and leads to significant changes of the spectrum of the gravity waves propagating upward. The efficiency of the wind filtering was found to be dependent on the solar cycle and season (Fritts & Vadas, 2008). This effect has been modeled by Sun et al. (2007) at the height of 300 km for a specific case. Our observations suggest that this wind-filtering mechanism is likely to be the dominant factor in the propagations of such disturbances at the middle latitudinal Ebro station during the daytime. The changes in the azimuthal directions of the ionospheric disturbances propagation has been reported earlier (e.g., Crowley et al., 1987; He et al., 2004; Lay et al., 2018; MacDougall et al., 2009); however, in most cases, only the analyzed datasets were limited in seasons, making it impossible to see the entire climatology TIDs and difference between the daytime and nighttime observations. We have not analyzed the seasonal behavior in the estimated TID azimuth directions due to the few years of data analyzed. However, we plan to do so in future as more data become available.

Hernández-Pajares et al. (2006) also reported a bimodal distribution of MSTIDs based on TEC observations over Europe. In their study, the first mode was observed around local noon time, and another one in the late evening hours. The modes had noticeably different azimuthal propagation angles: 150° for the noon-time

MSTIDs, and around 220° for the late evening ones. These results are in reasonable agreement with the full daily azimuthal distribution that is presented in Figure 9. The overall picture suggests that the daytime TIDs likely have tropospheric/mesospheric AGWs as the source, while the nighttime TIDs are possibly produced by the electric field disturbances, which is supported by the presence of the sporadic E layer during that period of time. Another possibility is that the dominant tilt azimuth of about 180° observed in Figure 9 for nighttime can be due to equatorward propagating LSTIDs originating in the auroral region. This is partially supported by the observations of the longer periodic variations during the night (Figure 6). Unfortunately, with single ionosonde tilt observations it is difficult to measure the spatial wavelengths of the observed disturbances to conclusively determine their origin. More observations within a larger ionosonde network are needed to address this question.

5. Summary and Conclusions

The ionospheric tilt concept provides another way of studying irregular ionospheric structure. Using the long-term observations at the Ebro digisonde station, it was found that the strongest disturbances in the observed ionospheric tilts are observed at the sunrise, when the tilt zenith angle can be as large as 3°. Spectral analysis with wavelets revealed the presence and exact periods of the wavelike disturbances that we associate with TIDs, which can be produced by AGWs or by electric field instabilities. The analyzed tilts were presented in terms of North-South and East-West components with the long-term biases and daily trends removed. Most of the observed TIDs periods are from 20–30 min to about 80 min, which are rather typical for MSTIDs.

Summertime appears to have the most frequent occurrence of disturbances in the tilts. Variations in ionospheric tilt intensity do not exhibit increase with the increase in solar activity, suggesting that most likely their origin is not geomagnetic disturbances. Most often TIDS are observed during the daytime, approximately between 08 and 16 UT, which is the period from shortly after the passage of the sunrise terminator, to before the sunset. Direction of propagation of the TIDs derived from the tilt measurements was also analyzed and compared to the neutral wind direction calculated with the TIEGCM model. There is a strong agreement between the TID azimuths and direction opposite to the neutral wind flow during the daytime. Overall, the most prominent direction of TID propagation rotates during the daytime by almost 180°, similarly to the rotation of the neutral wind direction modeled by TIEGCM. This is an indication that most of the observed daytime TIDs are likely to be produced by AGWs originating in the troposphere, and propagating upward into the ionosphere through the mesopause where the least affected are the waves propagating in the direction opposite to the background neutral wind. The nighttime events do not agree with the neutral wind direction, indicating that the nighttime disturbances are not of tropospheric origin, but more consistent with the electrified MSTIDs generation through Perkins instability scenario or with the LSTID generated by auroral activity.

There is also a good similarity between the sporadic E occurrence and TID presence, for most of the period of observations (Figure 8), except for December 2012, when some post sunset TID activity is observed, and the occurrence of the Es layer is rather marginal. For the nighttime period this agreement supports the mechanism of the interhemispheric E and F region link responsible for the generation of the electrified MSTIDs. It will be interesting to analyze digisonde skymap measurements at magnetically conjugated points to elaborate further on this mechanism. Other possibilities that are available from the use of the digisonde tilt measurements include running similar analysis for different geographic locations to establish a global pattern of the MSTIDs occurrence and propagation characteristics. It would be also interesting to run skymap/tilt measurements in conjunction with optical observations to compare disturbance signatures in HF and visual spectra. Earlier experiments have shown a great potential of simultaneous HF and optical observations (e.g., Joshi et al., 2017; Pedersen et al., 2011). Such study is planned for future work.

Acknowledgments
This research received support by Universitat Ramon Llull projects (2019-URL-Proj002 and 2019-URL-IR1rQ-002), with funds provided by "Secretaria d'Universitats i Recerca de la Generalitat de Catalunya" and "Obra Social la Caixa", and by grants PGC2018-096774-B-I00 (MCIU/AEI/FEDER, UE) and GA776011 (European Commission REA). The datasets used in this paper are available at https://osf.io/b2wy4/.

References

Angling, M. J., Shaw, J., Shukla, A. K., & Cannon, P. S. (2009). Development of an HF selection tool based on the electron density assimilative model near-real-time ionosphere. *Radio Science*, *44*, RS0A13. https://doi.org/10.1029/2008RS004022

Barnes, R. I., R. S. Gardiner-Garden, & Harris T. J. (2000). Real time ionospheric models for the Australian Defence Force. Workshops in Applications of Radio Science, http://www.sws.bom.gov.au/IPSHosted/NCRS/wars/wars2000/commg/barnes.pdf.

Batista, I. S., Abdu, M. A., Carrasco, A. J., Reinisch, B. W., de Paula, E. R., Schuch, N. J., & Bertoni, F. (2008). Equatorial spread F and sporadic E-layer connections during the Brazilian conjugate point equatorial experiment (COPEX). *Journal of Atmospheric and Solar-Terrestrial Physics*, *70*(8–9), 1133–1143.

Bauer, S. J. (1958). An apparent ionospheric response to the passage of hurricanes. *Journal of Geophysical Research*, *63*(1), 265–269. https://doi.org/10.1029/JZ063i001p00265

Bilitza, D., Altadill, D., Truhlik, V., Shubin, V., Galkin, I., Reinisch, B., & Huang, X. (2017). International Reference Ionosphere 2016: From ionospheric climate to real-time weather predictions. *Space Weather*, *15*, 418–429. https://doi.org/10.1002/2016SW001593

Bishop, R. L., Aponte, N., Earle, G. D., Sulzer, M., Larsen, M. F., & Peng, G. S. (2006). Arecibo observations of ionospheric perturbations associated with the passage of Tropical Storm Odette. *Journal of Geophysical Research*, *111*, A11320. https://doi.org/10.1029/2006JA011668

Cervera, M. A., & Harris, T. J. (2014). Modeling ionospheric disturbance features in quasi-vertically incident ionograms using 3-D magnetoionic ray tracing and atmospheric gravity waves. *Journal of Geophysical Research: Space Physics*, *119*(1), 431–440. https://doi.org/10.1002/2013JA019247

Cosgrove, R. B., & Tsunoda, R. T. (2004). Instability of the E-F coupled nighttime midlatitude ionosphere. *Journal of Geophysical Research*, *109*, A04305. https://doi.org/10.1029/2003JA010243

Crowley, G., Jones, T., & Dudeney, J. (1987). Comparison of short period TID morphologies in Antarctica during geomagnetically quiet and active intervals. *Journal of Atmospheric and Terrestrial Physics*, *49*(11), 1155–1162. https://doi.org/10.1016/0021-9169(87)90098-5

Daniell, R. E., Brown, L. D., Anderson, D. N., Fox, M. W., Doherty, P. H., Decker, D. T., et al. (1995). Parameterized ionospheric model: A global ionospheric parameterization based on first principle models. *Radio Science*, *30*(5), 1499–1510. https://doi.org/10.1029/95RS01826

Dao, E. V., McNamara, L. F., & Colman, J. J. (2016). Magnetic field effects on the accuracy of ionospheric mirror models for geolocation. *Radio Science*, *51*, 284–300. https://doi.org/10.1002/2015RS005884

Fritts, D. C., & Vadas, S. L. (2008). Gravity wave penetration into the thermosphere: Sensitivity to solar cycle variations and mean winds. *Annales de Geophysique*, *26*(12), 3841–3861. https://doi.org/10.5194/angeo-26-3841-2008

Galkin, I. A., Reinisch, B. W., Huang, X., & Bilitza, D. (2012). Assimilation of GIRO data into a real-time IRI. *Radio Science*, *47*, RS0L07. https://doi.org/10.1029/2011RS004952

Galushko, V. G., Paznukhov, V. V., Yampolski, Y. M., & Foster, J. C. (1998). Incoherent scatter radar observations of AGW/TID events generated by the moving solar terminator. *Annales Geophysicae*, *16*(7), 821–827. https://doi.org/10.1007/s00585-998-0821-3

Georges, T. M. (1968). HF Doppler studies of traveling ionospheric disturbances. *Journal of Atmospheric and Terrestrial Physics*, *30*(5), 735–746. https://doi.org/10.1016/S0021-9169(68)80029-7

He, L.-S., Dyson, P., Parkinson, M., & Wan, W. (2004). Studies of medium scale travelling ionospheric disturbances using TIGER SuperDARN radar sea echo observations. *Annales Geophysicae*, *22*, 4077–4088.

Hernández-Pajares, M., Juan, J. M., & Sanz, J. (2006). Medium-scale traveling ionospheric disturbances affecting GPS measurements: Spatial and temporal analysis. *Journal of Geophysical Research*, *111*, A07S11. https://doi.org/10.1029/2005JA011474

Hernández-Pajares, M., Juan, J. M., Sanz, J., Orus, R., Garcia-Rigo, A., Feltens, J., et al. (2009). The IGS VTEC maps: A reliable source of ionospheric information since 1998. *Journal of Geodesy*, *83*, 263–272. https://doi.org/10.1007/s00190-008-0266-1

Hocke, K. (1998). Phase estimation with the Lomb-Scargle periodogram method. *Annales Geophysicae*, *16*, 356–358.

Hocke, K., & Tsuda, T. (2001). Gravity waves and ionospheric irregularities over tropical convection zones observed by GPS/MET radio occultation. *Geophysical Research Letters*, *28*, 2815–2818. https://doi.org/10.1029/2001GL013076

Hooke, W. H. (1968). Ionospheric irregularities produced by internal atmospheric gravity waves. *Journal of Atmospheric and Terrestrial Physics*, *30*(5), 795–823. https://doi.org/10.1016/S0021-9169(68)80033-9

Huang, C. Y.-Y., Huang, Y., Su, Y.-J., Sutton, E. K., Hairston, M. R., & Coley, W. R. (2016). Ionosphere-thermosphere (IT) response to solar windforcing during magnetic storms. *Journal of Space Weather and Space Climate*, *6*, A4. https://doi.org/10.1051/swsc/2015041

Hung, T., Phan, R. J., & Phan Smith, R. (1978). Ionospheric Doppler sounder for detection and prediction of severe storms. *AIAAJ*, *16*(7), 763–766. https://doi.org/10.2514/3.60961

Jakowski, N., Mielich, J., Borries, C., Cander, L., Krankowski, A., Nava, B., & Stankov, S. M. (2008). Large-scale ionospheric gradients over Europe observed in October 2003. *Journal of Atmospheric and Solar - Terrestrial Physics*, *70*, 1856–1862. https://doi.org/10.1016/j.jastp.2008.01.015

Joshi, D., Groves, K. M., McNeil, W., Carrano, C., Caton, R. G., Parris, R. T., et al. (2017). HF propagation results from the Metal Oxide Space Cloud (MOSC) experiment. *Radio Science*, *52*(6), 710–722. https://doi.org/10.1002/2016RS006164

Kelley, M. C. (1997). In situ ionospheric observations of severe weather-related gravity waves and associated small-scale plasma structure. *Journal of Geophysical Research*, *102*, 329–335. https://doi.org/10.1029/96JA03033

Korepanov, V., Hayakawa, M., Yampolskic, Y., & Lizunovd, G. (2009). AGW as a seismo-ionospheric coupling responsible agent. *Physics and Chemistry of the Earth*, *34*, 485–495. https://doi.org/10.1016/j.pce.2008.07.014

Kozlov, A.V., & Paznukhov, V. V. (2008). Digisonde Drift Analysis Software. AIP Conference Proceedings. 974. 10.1063/1.2885026.

Lay, E. H., Parker, P. A., Light, M., Carrano, C. S., Debchoudhury, S., & Haaser, R. A. (2018). Midlatitude ionospheric irregularity spectral density as determined by ground-based GPS receiver networks. *Journal of Geophysical Research: Space Physics*, *123*, 5055–5067. https://doi.org/10.1029/2018JA025364

MacDougall, J., Li, G., & Jayachandran, P. (2009). Traveling ionospheric disturbances near London, Canada. *Journal of Atmospheric and Solar-Terrestrial Physics*, *71*(17-18), 2077–2084. https://doi.org/10.1016/j.jastp.2009.09.016

McNamara, L. F. (1991). *The ionosphere: Communications, surveillance, and direction finding*. Malabar, Fla: Krieger.

Munro, G. H. (1950). Travelling Disturbances in the Ionosphere, Proceedings of the Royal Society of London. *Series A*, *202*(1069), 208–223.

Munton, D., Rainwater, D., Gaussiran, T. L., Calfas, R. S., Reay, T. M., Schofield, J., & Fleischmann, A. (2019). A midlatitude HF propagation experiment over New Mexico. *Radio Science*, *54*, 298–313. https://doi.org/10.1029/2018RS006740

Narayanan, V. L., Shiokawa, K., Otsuka, Y., & Neudegg, D. (2018). On the role of thermospheric winds and sporadic E layers in the formation and evolution of electrified MSTIDs in geomagnetic conjugate regions. *Journal of Geophysical Research: Space Physics*, *123*, 6957–6980. https://doi.org/10.1029/2018JA025261

Obenberger, K. S., Dao, E., & Dowell, J. D. (2019). Experimenting with frequency-and-angular sounding to characterize traveling ionospheric disturbances using the LWA-SV radio telescope and a DPS4D. *Radio Science*, *54*, 181–193. https://doi.org/10.1029/2018RS006690

Paznukhov, V. V., Galushko, V. G., & Reinisch, B. W. (2012). Digisonde observations of TIDs with frequency and angular sounding technique. *Advances in Space Research*, *49*(4), 700–710. https://doi.org/10.1016/j.asr.2011.11.012

Pedersen, T., McCarrick, M., Reinisch, B., Watkins, B., Hamel, R., & Paznukhov, V. (2011). Production of artificial ionospheric layers by frequency sweeping near the 2nd gyroharmonic. *Annales de Geophysique*, *29*, 47–51.

Pradipta, R., Valladares, C. E., Carter, B. A., & Doherty, P. H. (2016). Interhemispheric propagation and interactions of auroral traveling ionospheric disturbances near the equator. *Journal of Geophysical Research, Space Physics*, *121*, 2462–2474. https://doi.org/10.1002/2015JA022043

Reinisch, B., Galkin, I., Belehaki, A., Paznukhov, V., Huang, X., Altadill, D., et al. (2018). Pilot ionosonde network for identification of traveling ionospheric disturbances. *Radio Science*, *53*(3), 365–378. https://doi.org/10.1002/2017RS006263

Reinisch, B. W., Galkin, I. A., Khmyrov, G. M., Kozlov, A. V., Bibl, K., Lisysyan, I. A., et al. (2009). New digisonde for research and monitoring applications. *Radio Science*, *44*, RS0A24. https://doi.org/10.1029/2008RS004115

Reinisch, B. W., Huang, X., Galkin, I. A., Paznukhov, V., & Kozlov, A. (2005). Recent advances in real-time analysis of ionograms and ionospheric drift measurements with digisondes. *Journal of Atmospheric and Solar-Terrestrial Physics*, *67*, 1054–1062. https://doi.org/10.1016/j.jastp.2005.01.009

Röttger, J. (1977). Travelling disturbances in the equatorial ionosphere and their association with penetrative cumulus convection. *Journal of Atmospheric and Terrestrial Physics*, *39*, 987–998. https://doi.org/10.1016/0021-9169(77)90007-1

Rovira-Garcia, A., Juan, J. M., Sanz, J., González-Casado, G., & Bertran, E. (2016). Fast precise point positioning: A system to provide corrections for single and multi-frequency navigation. *NAVIGATION, Journal of The Institute of Navigation*, *63*, 231–247. https://doi.org/10.1002/navi.148

Sauli, P., & Boska, J. (2001). Observations of gravity waves of meteorological origin in the F-region ionosphere. *Physics and Chemistry of the Earth, Part C: Solar, Terrestrial & Planetary Sci*, *26*, 425–428. https://doi.org/10.1016/S1464-1917(01)00024-1

Somsikov, V. M. (1987). A spherical model of wave generation in atmosphere by solar terminator. *Journal of Atmospheric and Terrestrial Physics*, *49*, 433–438. https://doi.org/10.1016/0021-9169(87)90037-7

Sun, L., Wan, W., Ding, F., & Mao, T. (2007). Gravity wave propagation in the realistic atmosphere based on a three-dimensional transfer function model. *Annales Geophysicae*, *25*, 1979–1986. https://doi.org/10.5194/angeo-25-1979-2007

Taylor, M. J., Ryan, E. H., Tuan, T. F., & Edwards, R. (1993). Evidence of pre-ferential directions for gravity wave propagation due to wind filtering in the middle atmosphere. *Journal of Geophysical Research*, *98*, 6047–6057. https://doi.org/10.1029/92JA02604

Vadas, S. L., & Crowley, G. (2010). Sources of the traveling ionospheric disturbances observed by the ionospheric TIDDBIT sounder near Wallops Island on 30 October 2007. *Journal of Geophysical Research*, *115*, A07324. https://doi.org/10.1029/2009JA015053

Waldock, J. A., & Jones, T. B. (1987). Source regions of medium scale travelling ionospheric disturbances observed at midlatitudes. *Journal of Atmospheric and Terrestrial Physics*, *49*, 105–114. https://doi.org/10.1016/0021-9169(87)90044-4

Yampolski, Y. M., Zalizovski, A. V., Litvinenko, L. M., Lizunov, G. V., Groves, K., & Moldwin, M. (2004). Magnetic field variations in Antarctica and the conjugate region (New England) stimulated by cyclone activity. *Radio Physics and Radio Astronomy*, *9*, 130. In Russian

Zalizovski, A. (2008). The role of tropospheric processes in forming the sporadic layers of E ionospheric region over the Antarctic peninsula. *Radiophysics and Radioastronomy*, *13*, 26–38.